
Proceedings Paper:
Colombo, M and Fairweather, M (2018) Two-Fluid Eulerian-Eulerian CFD Modelling of Bubbly Flows Using an Elliptic-Blending Reynolds Stress Turbulence Model. In: Proceedings of the 12th International ERCOFTAC Symposium on Engineering Turbulence Modelling and Measurements. ETMM12: 12th International ERCOFTAC Symposium on Engineering Turbulence Modelling and Measurements, 26-28 Sep 2018, Montpellier, France. ETMM.

TWO-FLUID EULERIAN-EULERIAN CFD MODELLING OF BUBBLY FLOWS USING AN ELLIPTIC-BLENDING REYNOLDS STRESS TURBULENCE MODEL

M. Colombo and M. Fairweather

School of Chemical and Process Engineering, University of Leeds, Leeds LS2 9JT, UK

M.Colombo@leeds.ac.uk

Abstract

In Eulerian-Eulerian two-fluid computational fluid dynamic (CFD) predictions of bubbly flows, the lateral void fraction distribution mainly results from a balance between the lift and wall lubrication forces. The impact of turbulence modelling on the void fraction distribution has not, however, been examined in detail. In this paper, this impact is studied with an elliptic blending Reynolds stress turbulence model (EB-RSM) that resolves the near-wall region and includes the contribution of bubble-induced turbulence. Lift and wall lubrication forces are deliberately neglected. Comparisons against data on bubbly flows in a pipe and a square duct show that the EB-RSM reproduces the lateral void fraction distribution, including the peak in the near-wall region. The accuracy of this approach is comparable to best-practice high-Reynolds k-ε and second-moment turbulence closures that include lift and wall lubrication contributions. Overall, the role of the turbulence field is demonstrated to be significant in determining void fraction distributions, and has to be modelled appropriately if more accurate and consistent modelling of bubbly flows is to be achieved. In view of this, the present EB-RSM approach is useful as a starting point to develop a more accurate and generally applicable set of closure models for two-fluid CFD approaches.

1 Introduction

In multiphase gas-liquid bubbly flows, the bubble size distribution and the volume fraction of the gas phase strongly affect the flow of the continuous liquid phase and the design and operation of industrial equipment. The use of computational fluid dynamic (CFD) models has made possible the calculation of three-dimensional void fraction and interfacial area distributions whilst accounting for phenomena at much smaller length scales (Rzehak and Krepper, 2013; Colombo and Fairweather, 2016). For the prediction of flows of industrial-scale, Eulerian-Eulerian averaged two-fluid models have been the most frequent choice (Hosokawa and Tomiyama, 2009; Colombo and Fairweather, 2015; Liao et al., 2015).

Eulerian-Eulerian two-fluid models treat the phases as interpenetrating continua and interphase exchanges are modelled by means of closure relations. In closed ducts, the tendency of smaller bubbles to migrate towards the walls and larger bubbles to concentrate towards the centre is attributed to the action of the lift force, with the change in direction in the region of bubble diameters from 4 to 6 mm (Lucas et al., 2010). Consequently, in most CFD studies to date, the lateral void fraction distribution essentially results from a balance between the lift and wall lubrication forces acting on the bubbles. Although over the years numerous lift models have been developed, and many have been optimized to predict the wall-peak void fraction distribution, no general consensus on the most accurate model has yet been reached (Hibiki and Ishii, 2007). Additionally, an even larger number of slightly different models is available for the wall lubrication force (Antal et al., 1991; Hosokawa and Tomiyama, 2009; Rzehak and Krepper, 2013; Colombo and Fairweather, 2015). However, more recently the near-wall peak of the void fraction profile was well-predicted even without lift and wall force contributions by using a near-wall Reynolds stress model (RSM) (Ullrich et al., 2014). With the exception of a small number of contributions (Lopez de Bertodano et al., 1990; Mimouni et al., 2010), the role of the continuous phase turbulence has been rarely considered in previous works, in which multiphase extensions of single-phase linear eddy viscosity models have generally been applied. However, recent direct numerical simulations (Santarelli and Frohlich, 2016) of fixed spherical bubbles in a shear flow found that, even with spherical bubbles, the lift force can become negative at high shear rates, demonstrating that the physical aspects of interfacial momentum transfer are more complex than generally envisaged. In addition, the presence of a liquid film between the bubble and the wall, which forms the basis of the wall lubrication theory, has also been questioned (Lubchenko et al., 2018).

In this paper, bubbly flows are predicted using a two-fluid Eulerian-Eulerian CFD model combined with a wall-resolved elliptic-blending Reynolds stress model (EB-RSM) of the turbulence. By neglecting lift and wall forces, the impact of the con-

tinuous phase turbulence on the lateral void fraction distribution is studied in a pipe and in a square duct, where the accuracy of lift and wall force models is much less well established. Results are compared to more standard high-Reynolds k-ε and Reynolds stress turbulence models. The action of the turbulence on the void fraction distribution and the benefits of high order turbulence modelling for overall two-fluid model accuracy and generality are addressed.

2 Numerical model

In the two-fluid Eulerian-Eulerian model, a set of averaged continuity and momentum conservation equations is solved for each phase (Prosperetti and Tryggvason, 2007; Yeoh and Tu, 2010). Turbulence is resolved in the continuous phase using the EB-RSM (Manceau, 2015) that allows solution of the turbulence field up to the near-wall region. The transport equations of the Reynolds stresses are based on the corresponding single-phase formulation, and the pressure-strain relation is modelled using the so-called "SSG model" (Speziale et al., 1991):

$$\begin{aligned}\Phi_{ij}^{h} = &-[C_{1a}\varepsilon + C_{1b}tr(P)]a_{ij} + \\ &C_2\varepsilon\left(a_{ik}a_{kj} - \tfrac{1}{3}a_{mn}a_{mn}\delta_{ij}\right) + \left[C_{3a} - \right. \\ &\left. C_{3b}\left(a_{ij}a_{ij}\right)^{0.5}\right]kS_{ij} + C_4k\left(a_{ik}S_{jk} + a_{jk}S_{ik} - \right. \\ &\left.\tfrac{2}{3}a_{mn}S_{mn}\delta_{ij}\right) + C_5\left(a_{ik}W_{jk} + a_{jk}W_{ik}\right)\end{aligned} \quad (1)$$

In the previous equation, k is the turbulence kinetic energy, ε the turbulence energy dissipation rate and a_{ij} the components of the anisotropy tensor. P is the turbulence production and S_{ij} and W_{ij} are the strain rate and the rotation rate tensors, respectively. Near the wall, the SSG model is blended with a formulation that reproduces the near-wall asymptotic behaviour of the turbulent stresses:

$$\begin{aligned}\Phi_{ij}^{w} = -5\frac{\varepsilon}{k}\Big[&\overline{u_iu_k}n_jn_k + \overline{u_ju_k}n_in_k \\ &- \frac{1}{2}\overline{u_ku_l}n_kn_l\left(n_in_j + \delta_{ij}\right)\Big]\end{aligned} \quad (2)$$

Transition from the near-wall model in Eq. (2) to weakly inhomogeneous behaviour away from the wall is ensured by the elliptic relaxation function α_{EB}, which is obtained by solving an elliptic relaxation equation:

$$\Phi_{ij} = (1 - \alpha_{EB}^3)\Phi_{ij}^{w} + \alpha_{EB}^3\Phi_{ij}^{h} \quad (3)$$

$$\alpha_{EB} - L\nabla^2\alpha_{EB} = 1 \quad (4)$$

where L is the turbulence length scale. More details on the EB-RSM formulation can be found in Manceau (2015). The bubble contribution to the continuous phase turbulence is accounted for with specific source terms that consider the conversion of energy lost by the bubbles to drag into turbulence kinetic energy in the bubble wakes (Rzehak and Krepper, 2013):

$$S_k^{BI} = K_{BI}\boldsymbol{F_d}\boldsymbol{U_r} \quad (5)$$

In Eq. (5), $\boldsymbol{F_d}$ is the drag force, $\boldsymbol{U_r}$ the relative velocity and K_{BI} is introduced to account for the modulation of the turbulence source. In the turbulence energy dissipation rate equation, the bubble-induced source is expressed as the corresponding turbulence kinetic energy source term multiplied by the timescale of the bubble-induced turbulence τ_{BI}:

$$S_\varepsilon^{BI} = \frac{C_{\varepsilon,BI}}{\tau_{BI}}S_k^{BI} \quad (6)$$

In multiphase turbulence, the bubble-induced turbulence timescale should be related to the shear-induced turbulent eddy lifetime as well as bubble length and velocity scales. The mixed timescale proposal from Rzehak and Krepper (2013) is adopted, where the velocity scale is derived from the square root of the liquid turbulence kinetic energy and the length scale from the bubble diameter. $C_{\varepsilon,BI}$ is fixed to 1 and K_{BI} is fixed to a value of 0.25, which provided good agreement over a large database of bubbly flows (Colombo and Fairweather, 2015). The bubble-induced turbulence model is implemented in the EB-RSM by splitting the contribution amongst the normal Reynolds stress components. The performance of the EB-RSM is compared against high-Reynolds number multiphase formulations of the k-ε and RSM turbulence models (CD-adapco, 2016).

For the interfacial momentum transfer closures, the drag force is accounted for with the model of Tomiyama et al. (2002) and the turbulent dispersion force with the approach of Burns et al. (2004). In the high-Reynolds number models, the lift force is also included using a constant value of the lift coefficient C_L = 0.1 (Colombo and Fairweather, 2015), and the wall force is modelled following Antal et al. (1991). As mentioned in the introduction, these two forces are neglected in the EB-RSM to highlight the impact of the turbulence field on the lateral void fraction distribution.

The models were solved using the STAR-CCM+ code (CD-adapco, 2016). Pipe flow was simulated in a two-dimensional axisymmetric geometry, whereas a 1/4 section of the square duct was employed. For the high Reynolds number turbulence models, a sensitivity study demonstrated that structured meshes (with 3000 and 129,375 cells, respectively) with the first grid point located close to y^+ = 30 were sufficient to obtain mesh-independent solutions. The EB-RSM requires a much more refined

mesh close to the wall. Mesh-independent solutions were achieved with grids having the centre of the first cell located at a non-dimensional wall distance of 1-1.5, and the number of cells equal to 20,800 and 1,280,000 for the pipe and duct flow, respectively.

At the inlet, constant phase velocities and void fractions were imposed, together with an imposed pressure at the outlet. The no-slip boundary condition was used at the wall. The average bubble diameter was considered constant and taken equal to average measurements from the Hosokawa and Tomiyama (2009), at 3.66 mm, and Sun et al. (2014), at 4.25 mm, experiments. Unfortunately, no additional detailed measurements of the average bubble diameter evolution and space distribution are available for the experiments considered. Second-order upwind schemes were used to discretize the convective terms. Strict convergence of residuals was ensured and the mass balance was checked to have an error always less than 0.1 % for both phases.

3 Results and discussion

In this section, numerical simulations are compared against experiment 4 of Hosokawa and Tomiyama (2009) in an air-water bubbly pipe flow, and the experiment at j_l = 0.75 m s^{-1} and j_a = 0.09 m s^{-1} in a square duct from Sun et al. (2014).

The void fraction radial profile predicted by the EB-RSM for the Hosokawa and Tomiyama (2009) experiment is shown in Figure 1, as a function of the non-dimensional radial distance from the wall r_w/R. The wall-peaked void fraction profile, which is a distinctive feature of bubbly flows in pipes, is obtained even if lift and wall lubrication forces are neglected. When this is the case, the steady momentum balance in the radial direction for the liquid phase reduces to:

$$\frac{\alpha_l}{\rho_l}\frac{\partial p}{\partial r} = \frac{F_{td,r}}{\rho_l} - \frac{\partial \alpha_l \overline{u_r u_r}^L}{\partial r} + \frac{\alpha_l}{r}\left(\overline{u_\theta u_\theta}^L - \overline{u_r u_r}^L\right) \tag{7}$$

A similar balance can be written for the gas phase. Combining the two and neglecting turbulence stresses in the gas phase in view of the very low density ratio in gas-liquid bubbly flows, the following equation governing the void fraction distribution is obtained:

$$\alpha_g \frac{\partial \alpha_g}{\partial r} = -\frac{F_{td,r}}{\rho_l \overline{u_r u_r}^L} + \frac{\alpha_g(1-\alpha_g)}{\overline{u_r u_r}^L}\left[\frac{\partial \overline{u_r u_r}^L}{\partial r} + \left(\frac{\overline{u_r u_r}^L - \overline{u_\theta u_\theta}^L}{r}\right)\right] \tag{8}$$

From Eq. (8), turbulence in the liquid phase impacts the void fraction distribution and is responsible for the preferential accumulation of bubbles near the wall. In more detail, the gradient in the liquid phase radial turbulent stress generates a corresponding radial pressure gradient in the flow (Figures 2 and 3) that pushes the bubbles towards the lower pressure region near the wall. There, pressure increases again approaching the wall as a consequence of the radial turbulent stress becoming zero. Therefore, although the wall force is neglected, further movement of the bubbles towards the wall is prevented and the wall-peaked void profile is obtained. Obviously, an accurate definition of the void fraction profile near the wall needs the turbulence field in that region to be finely resolved. To do so, a turbulence model able to resolve the flow field down to the viscous sub-layer is necessary.

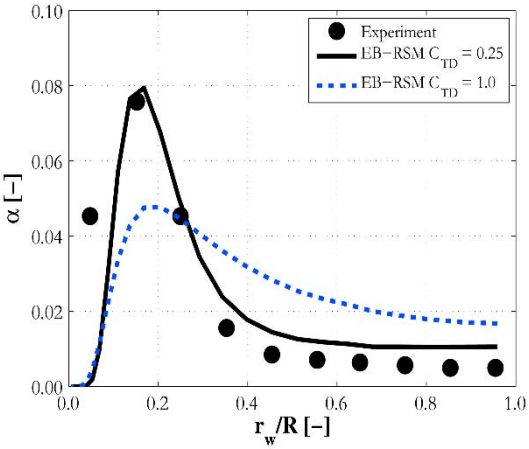

Figure 1: Radial void fraction profile compared with Hosokawa and Tomiyama (2009) experiment.

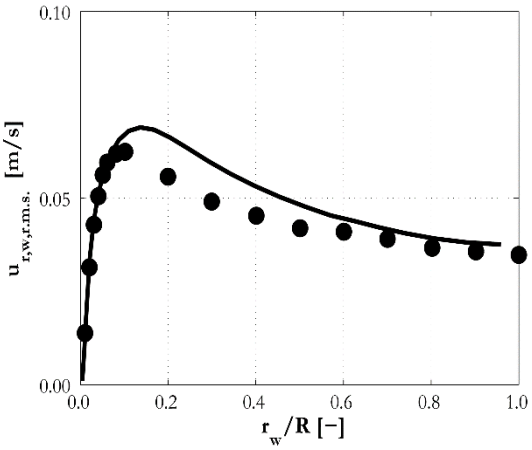

Figure 2: Radial profile of the r.m.s of the turbulent radial velocity fluctuations compared with Hosokawa and Tomiyama (2009) experiment.

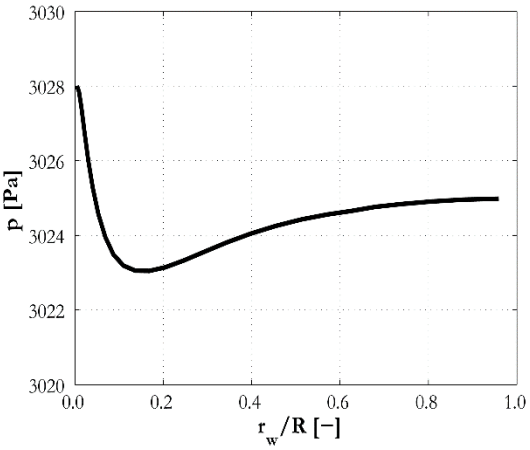

Figure 3: Calculated radial profile of the pressure field for the Hosokawa and Tomiyama (2009) experiment.

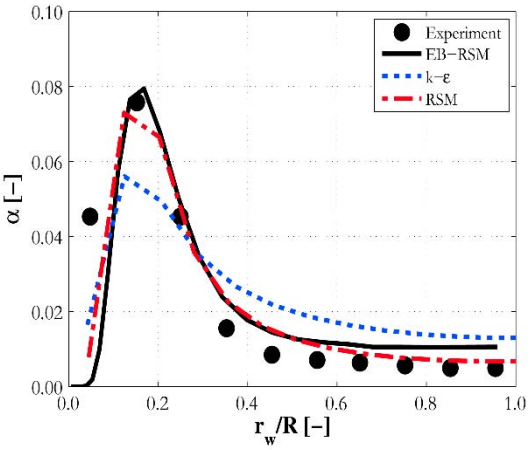

Figure 4: Radial void fraction profile compared with Hosokawa and Tomiyama (2009) experiment.

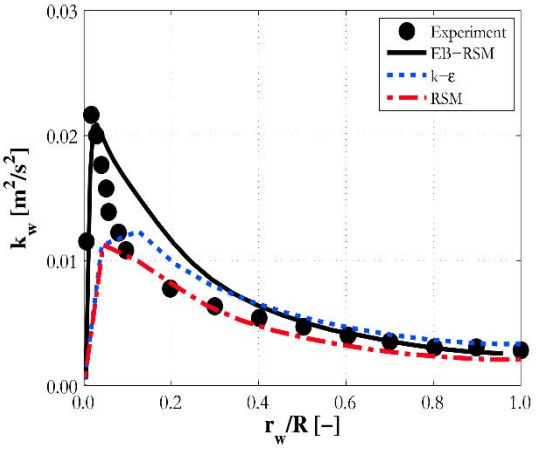

Figure 5: Radial profile of the turbulence kinetic energy compared with the Hosokawa and Tomiyama (2009) experiment.

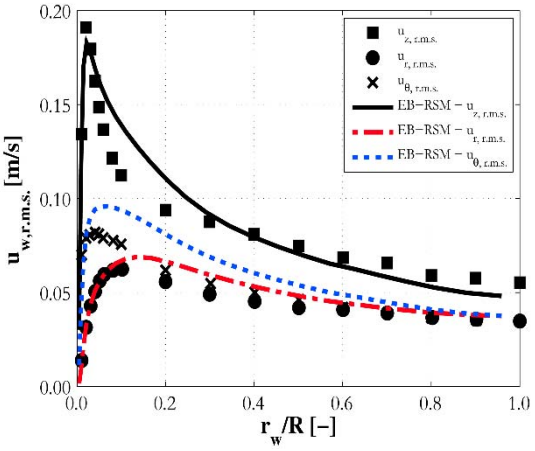

Figure 6: Radial profiles of the r.m.s. of the turbulent velocity fluctuations compared with the Hosokawa and Tomiyama (2009) experiment.

In Figure 1, the value of the peak is underestimated if the standard turbulent dispersion coefficient C_{TD} = 1.0 is used. Consequently, an excessive amount of void fraction is predicted in the centre of the pipe. More accurate predictions are obtained by reducing the turbulent dispersion coefficient to C_{TD} = 0.25. It is, however, important to point out that it is not suggested that the turbulent dispersion force be optimized on a case-by-case basis. In this paper, the objective is to highlight the impact of the turbulence model predictions on the void fraction distribution and, to do so, other radial forces have been neglected. However, the lift force will also have a significant impact, and it should not be neglected in any general CFD modelling of bubbly flows. Coupling the EB-RSM model with a proper lift force model will indeed be a primary objective of future work. In view of this, the use of a reduced C_{TD} illustrates that predictions using C_{TD} = 1.0 can be further improved by including additional radial forces such as lift.

Results from the EB-RSM are comparable with, and superior to, predictions obtained with the high-Reynolds number k-ε and Reynolds stress turbulence models (Figure 4), which include both lift and wall lubrication forces.

Figure 5 shows how predictions of the turbulence kinetic energy are improved near the wall when using the EB-RSM as compared to the high-Re formulations. Properly accounting for the bubble-induced contribution (Eqs. (5) and (6)) also leads to accurate predictions in the centre of the pipe. Figure 6 demonstrates the ability of the EB-RSM model to reproduce the anisotropy of the turbulence field and, therefore, the impact of the radial pressure gradient on the void fraction distribution.

Previous research has mostly focused on pipe flows, and it is therefore interesting to extend the present analysis to other less studied geometries, such as the square duct flow investigated experi-

mentally by Sun et al. (2014). The pressure distribution in the duct cross-section from the EB-RSM is shown in Figure 7, where a minimum in the corner of the duct is clearly visible. Similarly to what was reported for the pipe flow, the bubbles preferentially accumulate in this low pressure region and the void fraction distribution shows a maximum corresponding with the corner of the duct (Figure 8).

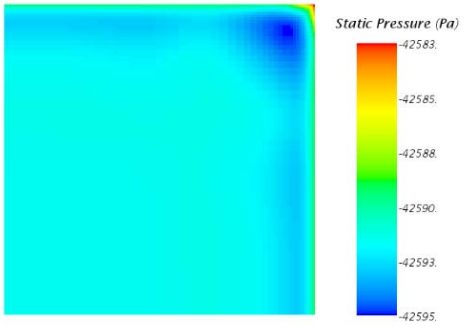

Figure 7: Pressure field for the Sun et al. (2014) experiment calculated with the EB-RSM.

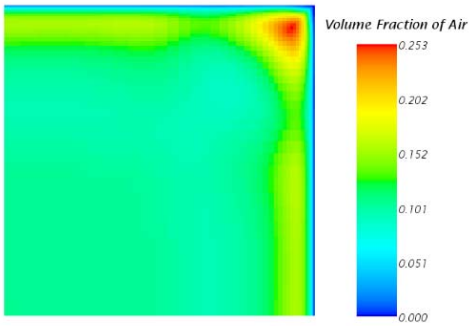

Figure 8: Void fraction field for the Sun et al. (2014) experiment calculated with the EB-RSM.

Figures 9 and 10 compare mean liquid velocity and void fraction predictions from the EB-RSM and the high-Reynolds number models. Figure 9 shows the liquid velocity profile on a line parallel to one of the lateral walls and as function of the non-dimensional distance from the perpendicular wall y_w/L. Good agreement is obtained with all the models, except for a small oscillation in the EB-RSM profile. This is probably due to an excessive sensitivity to the behaviour of the pressure field caused by the absence of any other radial forces. Figure 10 provides profiles of the void fraction along the diagonal of the duct and as a function of the non-dimensional distance from the duct corner d_w/D, where D is the diagonal length. Remarkably, the void fraction distribution is well-predicted by the EB-RSM. Therefore, although the model neglects any lift and wall lubrication contributions, the distinctive features of the void distribution, and the void peak in the corner of the duct, are correctly predicted by properly resolving the turbulence field and the near-wall region. Results are also in agreement with the high-Re number predictions, but the EB-RSM is the only model to predict the slight dip in the void fraction after the peak and the subsequent further increase towards the centre of the duct.

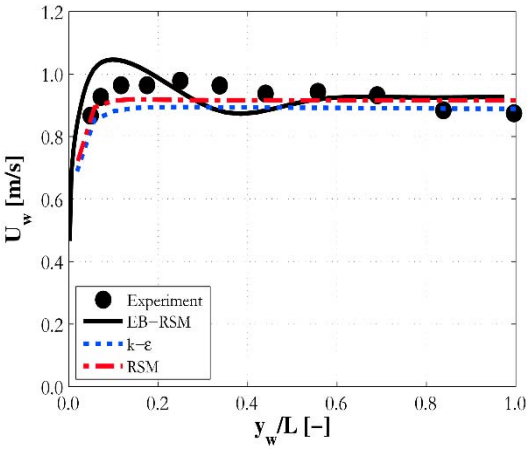

Figure 9: Liquid velocity predictions compared with the Sun et al. (2014) experiment.

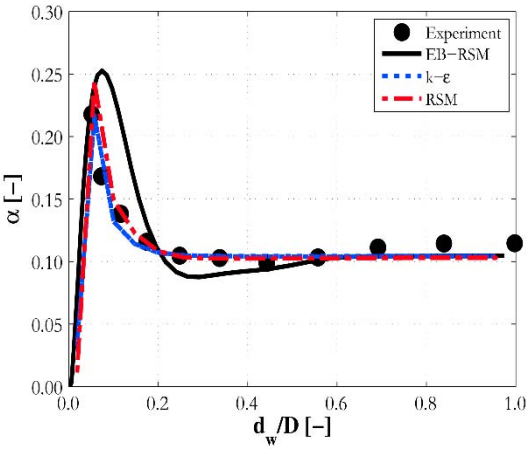

Figure 10: Void fraction predictions compared with the Sun et al. (2014) experiment.

3 Conclusions

The void fraction distribution and the main features of bubbly flows in a pipe and a square duct were well-reproduced by an Eulerian-Eulerian CFD two-fluid model. The model is closed with a EB-RSM and without accounting for lift and wall lubrication forces to highlight the action of the turbulence field on the lateral void distribution. The continuous phase turbulence field induces lateral pressure gradients that drive the void fraction distribution. Bubbles accumulate in low pressure regions near the wall of the pipe and the corner of the square duct, and wall-peaked void fraction distributions are well-predicted in both geometries. There-

fore, turbulence action has to be taken into account and reliably predicted and at least a second-moment turbulence closure that finely resolves the near-wall region is desirable. The lift force is still expected to play a prominent role and a proper lift model will be added in future work aimed at developing a two-fluid CFD model of improved accuracy and reliability.

Acknowledgements

The authors gratefully acknowledge the financial support of the EPSRC under grant EP/K007777/1, Thermal Hydraulics for Boiling and Passive Systems, and EP/M018733/1, Grace Time, part of the UK-India Civil Nuclear Collaboration.

References

Antal, S.P., Lahey, R.T. and Flaherty, J.E. (1991), Analysis of phase distribution in fully developed laminar bubbly two-phase flow, *Int. J. Multiphase Flow*, Vol. 17, pp. 635-652.

Burns, A.D., Frank, T., Hamill, I. and Shi, J.M. (2004), The Favre averaged drag model for turbulent dispersion in Eulerian multi-phase flows, *Fifth International Conference on Multiphase Flows*, Yokohama, Japan, May 30 - June 4.

CD-adapco (2016), STAR-CCM+® Version 10.04 User Guide.

Colombo, M. and Fairweather, M. (2015), Multiphase turbulence in bubbly flows: RANS simulations, *Int. J. Multiphase Flow*, Vol. 77, pp. 222-243.

Colombo, M. and Fairweather, M. (2016), RANS simulation of bubble coalescence and break-up in bubbly two-phase flows, *Chem. Eng. Sci.*, Vol. 146, pp. 207-225.

Hibiki, T. and Ishii, M. (2007), Lift force in bubbly flow systems, *Chem. Eng. Sci.*, Vol. 62, pp. 6457-6474.

Hosokawa, S. and Tomiyama, A. (2009), Multi-fluid simulation of turbulent bubbly pipe flow, *Chem. Eng. Sci.*, Vol. 64, pp. 5308-5318.

Liao, Y., Rzehak, R., Lucas, D. and Krepper, E. (2015), Baseline closure model for dispersed bubbly flow: Bubble coalescence and breakup, *Chem. Eng. Sci.*, Vol. 122, pp. 336-349.

Lopez de Bertodano, M., Lee, S.J., Lahey Jr., R.T. and Drew, D.A. (1990), The prediction of two-phase turbulence and phase distribution phenomena using a Reynolds stress model, *J. Fluid Eng.*, Vol. 112, pp. 107-113.

Lubchenko, N., Magolan, B., Sugrue, R. and Baglietto, E. (2018), A more fundamental wall lubrication force from turbulent dispersion regularization for multiphase CFD applications, *Int. J. Multiphase Flow*, Vol. 98, pp. 36-44.

Lucas, D., Beyer, M., Szalinski, L. and Schutz, P. (2010), A new database on the evolution of air-water flows along a large vertical pipe, *Int. J. Therm. Sci.*, Vol. 49, pp. 664-674.

Manceau, R. (2015), Recent progress in the development of the elliptic blending Reynolds-stress model, *Int. J. Heat Fluid Flow*, Vol. 51, pp. 195-220.

Mimouni, S., Archambeau, F., Boucker, M., Lavieville, J. and Morel, C. (2010), A second order turbulence model based on a Reynolds stress approach for two-phase boiling flows. Part 1: Application to the ASU-annular channel case, *Nucl. Eng. Des.*, Vol. 240, pp. 2233-2243.

Prosperetti, A. and Tryggvason, G. (2007), Computational methods for multiphase flow, Cambridge University Press, Cambridge, United Kingdom.

Rzehak, R. and Krepper, E. (2013), CFD modelling of bubble-induced turbulence, *Int. J. Multiphase Flow*, Vol. 55, pp. 138-155.

Santarelli, C. and Frohlich, J. (2016), Direct numerical simulations of spherical bubbles in vertical turbulent channel flow, *Int. J. Multiphase Flow*, Vol. 81, pp. 27-45.

Speziale, C.G., Sarkar, S. and Gatski, T.B. (1991), Modelling the pressure-strain correlation of turbulence: An invariant dynamical system approach, *J. Fluid Mech.*, Vol. 227, pp. 245-272.

Sun, H., Kunugi, T., Shen, X., Wu, D. and Nakamura, H. (2014), Upward air-water bubbly flow characteristics in a vertical square duct, *J. Nucl. Sci. Technol.*, Vol. 51, pp. 267-281.

Tomiyama, A., Celata, G.P., Hosokawa, S. and Yoshida, S. (2002), Terminal velocity of single bubbles in surface tension dominant regime, *Int. J. Multiphase Flow*, Vol. 28, pp. 1497-1519.

Ullrich, M., Maduta, R. and Jakirlic, S. (2014), Turbulent bubbly flow in a vertical pipe computed by an eddy-resolving Reynolds stress model, *10th International ERCOFTAC Symposium on Engineering Turbulence Modelling and Measurements* (*ETMM 10*), Marbella, Spain, September 17-19.

Yeoh, G.H. and Tu, J.Y. (2010), Computational techniques for multiphase flows – Basics and applications, Butterworth-Heinemann, Elsevier, Oxford, United Kingdom.